NANO LETTERS

Letter

pubs.acs.org/NanoLett

Plasmonic Whispering Gallery Cavities As Optical Nanoantennas

Ernst Jan R. Vesseur* and Albert Polman

Center for Nanophotonics, FOM Institute AMOLF, Science Park 104, 1098 XG Amsterdam, The Netherlands

ABSTRACT: We study the resonant modes of surface plasmon whispering gallery cavities based on a circular groove in a Au surface. We use spatially, angle-, and polarization-resolved cathodoluminescence spectroscopy to measure the resonant plasmonic local field distribution at deep-subwavelength resolution and determine the far-field radiation distribution for each plasmonic mode. We show mode-selective excitation of the plasmonic modes and resolve the modal angular radiation pattern. The results show that plasmonic whispering gallery resonators can be used as versatile antennas both in receiving and transmitting mode.

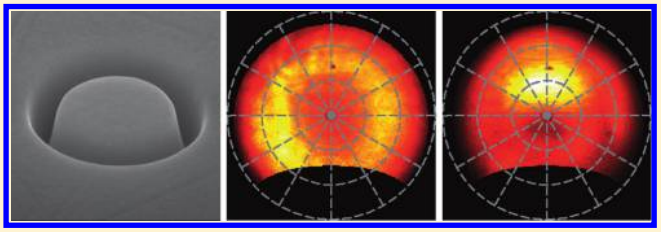

KEYWORDS: *Plasmon, ring antenna, cathodoluminescence spectroscopy, angle-resolved*

Optical nanoantennas provide an interface between the optical near field and far field.[1] Optical antennas coupled to optical emitters can cause strong modification in the spontaneous emission rate,[2−5] polarization,[6] and angular distribution of the light.[4,7,8] Conversely, in the receiving mode optical nanoantennas concentrate light from far-field illumination into a small volume, enlarging the effective absorption cross section of molecules, quantum dots, or atomic emitters placed near the antenna, or concentrating energy into a small detector.[9]

So far, most studies of antenna-emitter coupling have focused on single metal nanoparticles with shapes varying from spheres[3,10] to elongated nanorods,[11,12] and coupled nanoparticle geometries such as two coupled nanorods,[13−17] or arrays of metal nanoparticles.[18−22] All these geometries take advantage of the fact that light is concentrated in a localized mode with high absorption or emission cross section due to the high polarizability at the metal plasmon resonance.

Here, we introduce a ring resonator in a planar Au surface as a novel optical nanoantenna geometry that provides unique control over the near-to-far-field coupling. The circular groove sustains surface plasmon resonances that are due to groove-bound surface plasmon polaritons that are confined between the two closely spaced groove sidewalls.[23] Resonances occur when the circumference of the ring equals an integer number m of plasmon wavelengths. The lowest order azimuthal resonance in these plasmonic whispering gallery cavities occurs if the ring circumference equals a single plasmon wavelength λ. As we have shown previously,[24] these plasmon ring cavities also support many high-order azimuthal modes for increasing diameter. In addition, for deeper grooves, higher-order radial modes (with mode number n) are observed that correspond to an increase in the number of antinodes in the radial direction of the cavity.

The large degree of control over the mode field symmetries of the plasmon whispering gallery resonators provides a unique way to control the coupling between the near and far field. Also, due to the relatively large mode volume, these antennas can couple to a large volume of optical emitters. However, to exploit these features detailed knowledge of the spatial distribution of these modes and their angular emission pattern is required. This information cannot be obtained using conventional techniques. In this paper, we use a new technique, angle-resolved cathodoluminescence imaging spectroscopy in combination with white light scattering to study this behavior. This technique uses excitation in the near field by fast electrons to selectively excite well-defined antenna modes by tuning the position of excitation. The angular distribution and polarization of the antenna emission is tuned by the resonant mode order.

These experiments show that plasmonic whispering gallery cavities are ideal structures in which the radial and azimuthal mode symmetries of the resonant near field can be precisely tuned leading to accurate control over the coupling between near and far field. Interestingly, while the azimuthal modes are due to cavity resonance of propagating surface plasmon resonances, they can be well described by mode field symmetries of dipolar, quadrupolar, and higher order localized modes.

Arrays of plasmonic whispering gallery resonators were fabricated using focused-ion-beam milling. The resonators consist of a circular groove milled into a smooth Au surface. A representative structure is shown in Figure 1. The V-shaped grooves are approximately 100 nm wide at the top with a depth d ranging from 25 to 500 nm. Ring radii r are in the range 100−300 nm. The substrate was obtained by thermal evaporation of a thick (3 μm) Au layer onto a freshly cleaved mica substrate. After annealing at 500 °C, it was glued to a silicon wafer using an epoxy resin (EPO-TEK 377), cured at 150 °C, and subsequently stripped off the mica template. The resulting film

Received: September 30, 2011
Revised: November 16, 2011
Published: November 30, 2011

dx.doi.org/10.1021/nl203418c | *Nano Lett.* 2011, 11, 5524–5530

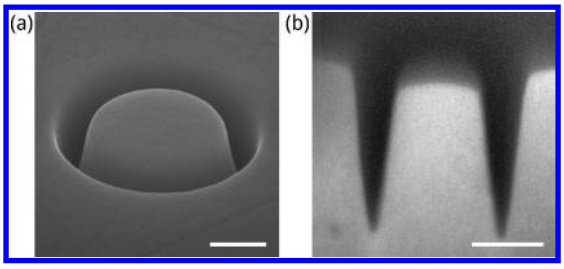

Figure 1. (a) Scanning electron micrograph of plasmonic whispering gallery resonator with radius r = 300 nm and groove depth d = 500 nm. (b) FIB-milled cross section through a resonator infilled with a protective Pt layer. Scale bars: 200 nm.

has a very smooth surface composed of large (~10 μm) crystal domains.

Cathodoluminescence (CL) measurements were taken in an FEI XL30 SEM using 30 keV electrons. A parabolic mirror placed in the SEM chamber collects the light emitted from the sample and guides it into a spectrometer equipped with a liquid-nitrogen-cooled CCD array detector, as is shown in Figure 2a. Ring resonators were excited by scanning the electron beam (current ~1 nA) over a 900 nm long line across the ring in 10 nm steps with an exposure time of 0.25 s per step. For each beam position, a spectrum was recorded. Spectra taken along a single line scan were summed to yield an integrated spectrum of the resonator.

White-light scattering measurements were taken using a 60× NA = 0.9 objective focusing white light from an incandescent lamp source onto the sample surface. Scattered light was collected by the same objective and, using a beam splitter, projected onto a 9 μm core diameter fiber guiding the light into a spectrometer equipped with a thermoelectrically cooled CCD array detector.

Ring resonances can both be excited by an incoming plane wave and by an incoming electron beam; however the mechanisms of excitation are different. We compare the scattering spectrum with the CL emission spectrum and use the differences between these spectra to study the mode symmetries.

Figure 3 shows the scattering and CL spectra of three representative rings with radii of 100, 210, and 290 nm and a depth of approximately 100 nm. For the smallest ring with a 100 nm radius, the CL spectrum (black curve) shows one clear peak. In contrast, the white-light scattering spectrum for this ring (red curve) is featureless. As known from previous work[23] the CL emission peak for a small ring of 100 nm radius is

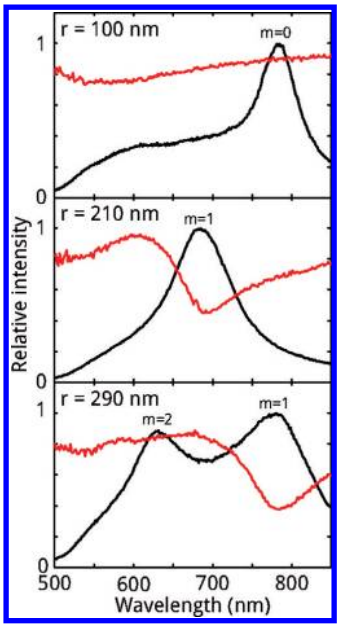

Figure 3. White-light scattering spectra (red curves) and 30 keV cathodoluminescence spectra (black curves) of ring resonators with increasing radius r. Resonances give rise to peaks in the cathodoluminescence spectra and Fano-type line shapes in the scattering spectra. All optical resonances (m = 0, 1, 2) are excited by the electron beam, but only dipolar (m = 1) resonances are excited in the white-light scattering experiment.

caused by a resonance with an m = 0, n = 1 symmetry, which corresponds to a charge distribution that is symmetric around the ring; the modal charge distribution has a vertical dipole moment. Such resonances are efficiently excited by an electron beam incident from the top, parallel to the dipole moment,[25] which is in agreement with the clear emission peak observed in the CL spectrum. Light that is incident through an objective, on the other hand, offers an electric field that is mostly polarized in the sample plane and thus perpendicular to the resonator modal field. This explains why the excitation is not visible in the scattering spectrum.

For the second ring (r = 210 nm), the m = 0 peak has shifted to a longer wavelength outside the measurement range and another peak is clearly visible at 675 nm in the CL spectrum. At this wavelength, the white-light scattering spectrum shows a dip. This corresponds to the excitation of an m = 1 resonance that has a dipolar charge distribution in the plane of the ring resonator. Both the incoming electron and a plane wave couple

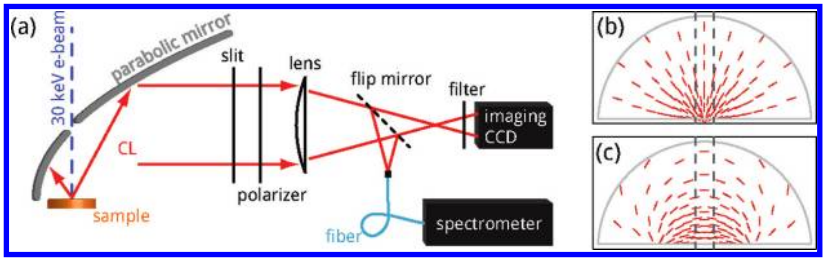

Figure 2. (a) Schematic of the cathodoluminescence imaging spectroscopy setup (not to scale). Cathodoluminescence emission from a sample, caused by an impinging 30 keV electron beam, is collected by a parabolic mirror placed above the sample. The light is guided toward a detection system that includes a camera to directly monitor the beam and a spectrometer equipped with a CCD array detector. (b) Polarization at different positions in the beam for a dipole emitter in the focus of the parabolic mirror aligned with the axis of the paraboloid (dipole perpendicular to the plane of the figure). Dashed lines indicate the area selected by a slit in polarized-spectroscopy mode. (c) Same as in (b) for a dipole emitter with horizontal orientation perpendicular to the optical axis (dipole pointing from left to right in the figure).

dx.doi.org/10.1021/nl203418c | Nano Lett. 2011, 11, 5524–5530

to this resonance. Although the resonant dipole moment is perpendicular to the electron beam, the modal electric field vector has vertical components in significant parts of the resonator groove[23] resulting in excitation of the resonance.

The CL spectrum of the largest ring (r = 290 nm) shows two peaks. Here, the scattering spectrum only shows a feature at the wavelength of the rightmost peak. This peak at 780 nm corresponds to the m = 1 mode[23] also observed in the r = 210 nm ring, now shifted to a longer wavelength due to the increased size of the resonator. The peak at 625 nm corresponds to an m = 2 resonance with a quadrupolar charge distribution. As with the dipolar m = 1 mode, this quadrupole mode is efficiently excited by the electron beam at positions where its near field has a large vertical component. Quadrupolar charge distributions are often disregarded when considering far-field radiation. This is valid when the oscillating charges are confined in a deep subwavelength volume. Here, however, the charges are distributed over wavelength-scale dimensions of the whispering gallery cavity and far-field emission is indeed observed under electron excitation. In contrast, such a quadrupolar oscillation does not couple to a plane wave incident from the top for symmetry reasons analogous to the m = 0 case. Indeed, there is no signature of the m = 2 resonance in the scattering spectrum.

In the comparison between CL and scattering, another interesting feature is observed. The peaks in the CL spectra have an apparent Lorentzian line shape, as is expected for this resonant behavior, whereas the dips in the white-light scattering spectra are asymmetric. This difference is attributed to interference between directly reflected light and radiation by the resonant mode. At an excitation wavelength below resonance, the resonator oscillates out of phase (phase shift is close to π) with the driving field, that is, the incident light. The incident light itself undergoes a phase shift of $\sim\pi$ upon direct reflection off the substrate. These effects combined cause constructive interference of the two light paths, leading to an enhanced scattering signal at wavelengths shorter than the resonance wavelength. Above the resonance wavelength, the phase shift upon reflection remains π, however the resonator now oscillates in phase with the driving field, leading to destructive interference between directly reflected light and light that is coupled out of the resonator. Indeed, at longer wavelengths a decreased scattering intensity is observed. This Fano-type interference[26] between a continuum and a single resonance that leads to this line shape is a well-known phenomenon in plasmonic resonances.[27]

Next, we take advantage of the deep subwavelength resolution of the CL technique to investigate the spatial distribution of the plasmonic modes and their coupling to far-field radiation. We use the unique capability of our CL system to collect also the angle- and polarization-resolved emission.

Because of the rotational symmetry of the ring resonators, the different multipolar fields are two-fold degenerate. This degeneracy can be lifted by analyzing the CL emitted from the resonator through a polarizing plate. The CL setup (see Figure 2a) allows for the placement of a polarizer in the part of the beam that emerges from the parabolic mirror.

When placing the polarizer after the parabolic mirror, it is important to take into account the effects of the mirror on the polarization. Figure 2b,c shows the polarization at several positions in the beam resulting from a dipole radiating in the mirror focus. As a result of reflection by the mirror, the polarization is turned by different angles in different positions in the beam. Along a vertical line through the center of the beam, the polarization is always identical, as Figure 2b,c shows for two different polarizations. In our setup, light is collected through a vertical slit positioned in the center of the beam. When analyzing this light with a polarizer, a single polarization emitted from the mirror focus is selected. The slit was 0.9 mm wide (less than 1/20 of the beam width) and the polarizer was set to either horizontal or vertical orientation. In polarized-emission experiments, the electron beam was scanned in a rectangular grid of 10 nm steps using a 0.1 s exposure time per pixel. For every pixel, a spectrum was acquired.

Angle-resolved measurements were taken without the slit, collecting light from the full area of the mirror, while the electron beam was fixed to one position on the resonator. The resonant mode was selected using band-pass filters with a 40 nm bandwidth around the wavelength of interest. Data is collected by a CCD array detector placed in the parallel beam that leaves the parabolic mirror. In this beam, every position corresponds to a unique emission angle. The CCD data was converted to an angular distribution.[28,29] The exposure time was 6 s.

Figure 4d–o shows CL data taken from two different ring resonators with r = 120 nm (Figure 4a) and r = 300 nm (Figure 4b,c). The groove depth was d = 100 nm in both cases. The left column shows CL data for the m = 0 resonance of the small ring at 750 nm. For this resonance the phase is constant throughout the groove and the dipole moment is oriented perpendicular to the sample surface. The center and right columns show CL data for the m = 1 resonance at 770 nm and the m = 2 resonance at 630 nm for a larger ring that correspond to one or two plasmon wavelengths fitting in the ring circumference, respectively.

Figure 4d–f show spatially dependent cathodoluminescence excitation maps for the m = 0, 1, 2 resonances. The data in Figure 4d is taken at the peak resonant wavelength of 750 nm. Data for the m = 1 and 2 resonances in Figure 4e,f is taken at λ_0 = 600 and 800 nm, respectively, to avoid overlap between the resonant peaks. Data taken with unpolarized detection (second row) shows circular features for all resonances, which is expected for a rotationally symmetric structure with accordingly degenerate modes. Interestingly, the m = 0 resonance in Figure 4d is mostly excited at the center of the ring. This is in agreement with the m = 0 mode symmetry and a vertical dipole moment, which is efficiently excited in the center of the structure. The m = 1, 2 resonances in (e) and (f) are best excited at the edges of the center plateau because the resonant field for these modes is strongest inside the groove. The strongest excitation is observed on the inner edges of the groove, as here the out-of-plane component of the modal field, which couples efficiently with the field of the electron beam, has a maximum.[23]

The third row of Figure 4 shows CL scans acquired through a slit with a polarizer transmitting vertically polarized light. The m = 0 dipole mode is expected to emit a rotationally symmetric radiation pattern with a polarization that is perpendicular to the sample surface. This emission is readily transmitted through the polarizer. Indeed, the excitation map Figure 4g at 750 nm is very similar to the unpolarized case, consistent with the dipole moment being vertical to the sample surface. The data for the m = 1 resonance in Figure 4h, also taken through the polarizer is very different. Here the rotational symmetry is lost and two lobes are clearly visible. This behavior is attributed to an in-plane dipole moment of which we only detect the far-field

dx.doi.org/10.1021/nl203418c | Nano Lett. 2011, 11, 5524–5530

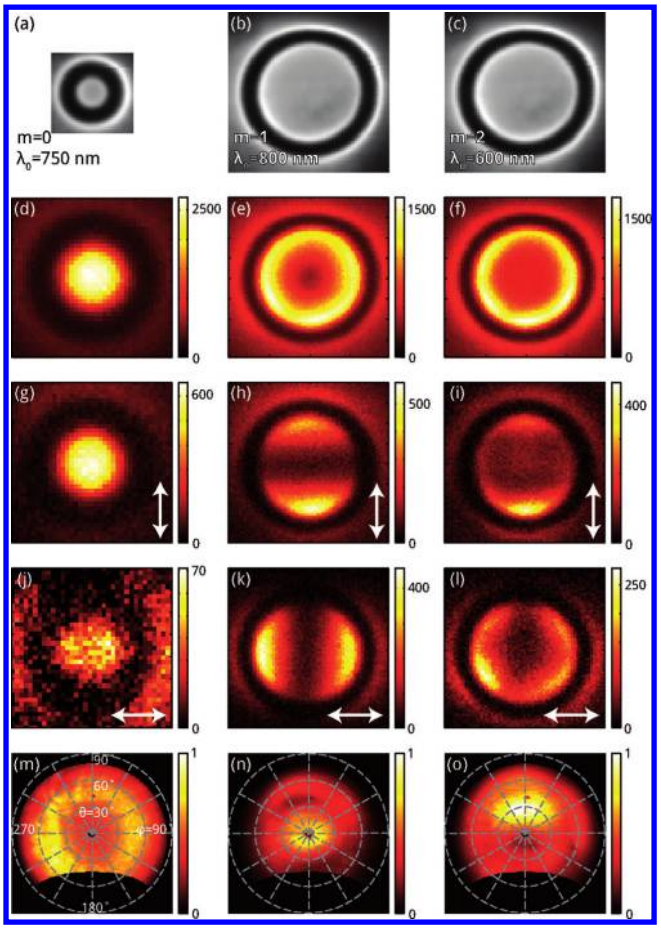

Figure 4. Spatially resolved excitation and angle-resolved emission of m = 0, 1, 2 resonances in plasmonic whispering gallery resonators. Left column (a–d) m = 0; data for an r = 120 nm ring resonator at a wavelength of 750 nm. Image size: 400 × 400 nm^2. Center column (b–k): m = 1; data for an r = 200 nm ring resonator at 800 nm wavelength. Image size: 800 × 800 nm^2. Right column (c–l): m = 2; data for the same r = 200 nm ring resonator at 600 nm wavelength with the same image size. First row: Scanning electron micrographs. Second row to fourth row: e-beam excitation maps (30 keV e$^-$), acquired using unpolarized detection, vertical polarization, and horizontal polarization, respectively. Color scales indicate CCD counts. The arrows indicate the orientation of the polarizer. Fifth row: angle-resolved emission of the resonant mode for excitation in the center of the resonator (m) and excitation at the bottom edge of the center plateau of the resonator (n) and (o).

radiation through the polarizer if it is excited with the matching polarization. The vertical polarization is only excited when the electron beam dwells near the top or the bottom of the resonator in the image of Figure 4b, where the maxima in the CL image of Figure 4h are observed. The data for the m = 2 resonance in Figure 4i are more complex; the image shows that this mode is mostly excited near the top and the bottom but there is a nonzero excitation around the full circumference of the ring. The excitation map for a quadrupolar resonance is indeed expected to be more complex than that of a dipole; we will clarify this result later. The small intensity in the center of Figure 4i is attributed to an m = 0, n = 2 resonance that overlaps with the signal at 600 nm.[23]

The excitation maps collected through the vertical slit drastically change when the polarizer is rotated to a horizontal orientation (fourth row). The m = 0 dipole mode does not emit the corresponding polarization and indeed, the signal in Figure 4j is very low. The small intensity that is transmitted is attributed to a dipolar mode also present in this structure with its maximum at a much shorter wavelength. In Figure 4k, the dipolar pattern of the m = 1 image now has the high-intensity lobes on the left and the right of the image, as is expected. The quadrupolar m = 2 mode (Figure 4l) shows four clear lobes with maxima that are rotated by 45° with respect to the vertical-polarization-scan.

Angle-resolved measurements without polarizer were taken to verify the conclusions made about the dipole orientations of the m = 0 and m = 1 resonances as well as to clarify the patterns observed for the quadrupolar m = 2 resonance. The fifth row of Figure 4 shows the angular emission patterns for a half sphere covering the ring resonator; azimuthal angle φ and polar angle θ are indicated. The black area in the bottom of each image corresponds to the open part of the parabolic mirror, where no light is collected. The orientation of the angular plots corresponds to that of the excitation maps. Figure 4m shows the emission owing to excitation of the m = 0 resonance on the center plateau. A bright ring is observed, indicating azimuthally symmetric emission into all directions. The polar angle of maximum intensity is around 45°. This angular emission pattern is in agreement with what is expected for a vertical dipole (λ = 750 nm) oscillating at the Au–air interface and is similar to the angular distribution of transition radiation.[30] Figure 4n shows the angular distribution for the m = 1 dipole emission. Here the beam was placed at the bottom edge of the center plateau (position of maximum intensity in (h)). For a dipole oriented parallel to the sample surface and vertically in these figures, a horizontal emission band is expected through the center of the angular plot, but due to the presence of the Au surface, this band should be truncated at shallow angle, resulting in emission that is mostly upward.[31] The figure indeed shows maximum intensity in the center of the distribution, corresponding to upward emission. The upward emission is always transmitted by the slit used for polarized measurements, independent of the orientation of the m = 1 dipole mode. This is in agreement with the fact that the signal intensities in Figure 4h,k are comparable.

Figure 5 shows the angular emission pattern of the m = 1 resonance for several electron beam positions around the ring circumference. The center image shows the excitation map of the resonator at 800 nm for a coarse scan of the electron beam. For each pixel, the angular emission was recorded and the pixel intensity represents the integrated angular emission. The angular emission patterns are plotted for eight selected pixels on the ring circumference. The results confirm that the observation of upward emission from the m = 1 mode is independent of electron beam position.

The emission pattern of the m = 2 quadrupole mode (also excited at the bottom of the ring) is given in Figure 4o. A bright spot is emitted at ~30° from the normal in a direction opposite the electron beam position. The signal has a minimum at the center of the plot, and a slightly higher intensity toward the bottom. Although the m = 2 resonance is a lateral or square quadrupole mode, this emission pattern, having a node in the center, reminds of the pattern of a linear quadrupole with a vertical orientation.[32,33] For a vertically oriented linear quadrupole the emitted polarization is also vertical. By comparing excitation maps Figure 4i,l it is found that for excitation at the bottom edge of the center plateau the emission indeed has a predominantly vertical polarization, which is in

dx.doi.org/10.1021/nl203418c | Nano Lett. 2011, 11, 5524–5530

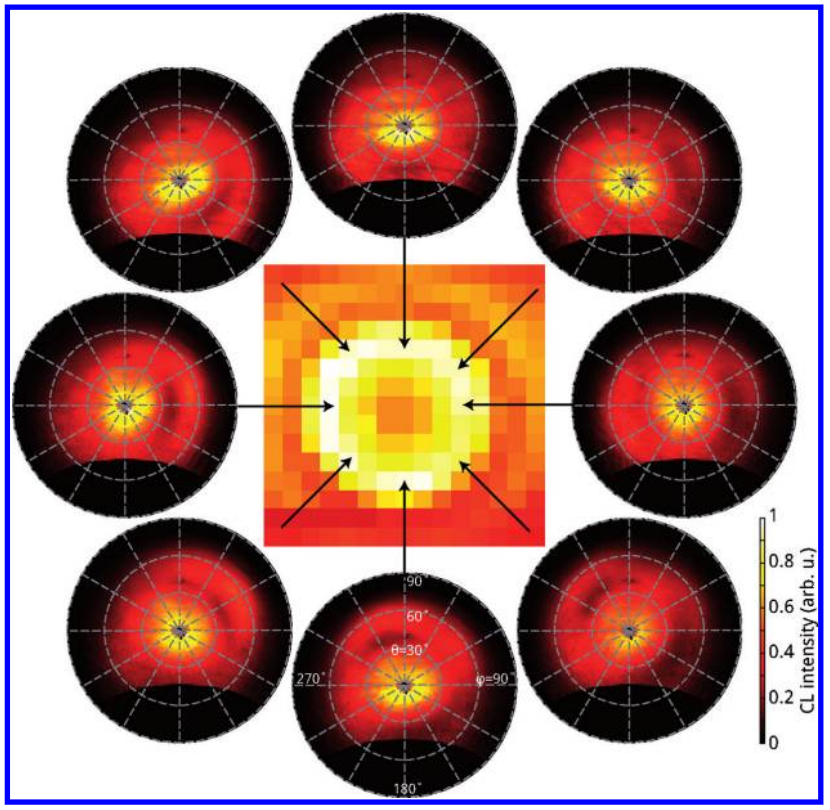

Figure 5. Angle-resolved emission from the m = 1 dipolar mode of an r = 300 nm, d = 100 nm ring resonator. Center: excitation map at 800 nm of the dipolar plasmon mode. For selected pixels on the inner edge of the center plateau, the angular emission pattern is plotted. The figure shows that the dipolar resonance always radiates toward the surface normal, independent of electron beam position.

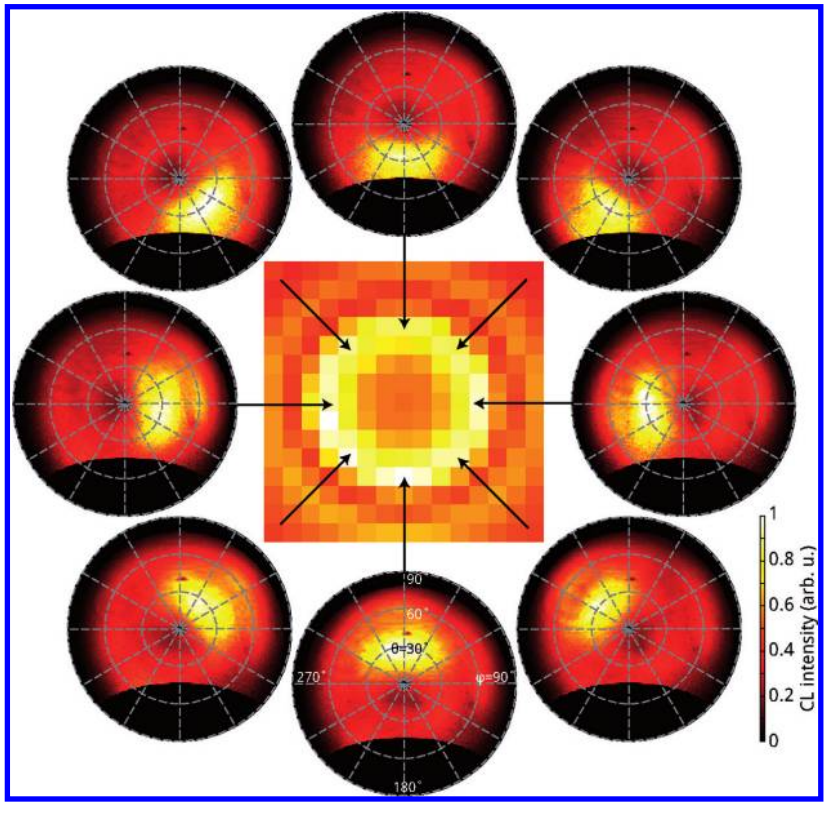

Figure 6. Angle-resolved emission from the m = 2 quadrupolar mode of an r = 300 nm, d = 100 nm ring resonator. Center: excitation map at 600 nm. For selected pixels on the inner edge of the center plateau, the angular emission pattern is plotted, showing a maximum in emission that is 30° from the normal and pointing in a direction opposite the electron beam position.

dx.doi.org/10.1021/nl203418c | *Nano Lett.* 2011, 11, 5524–5530

agreement with the linear quadrupole picture. However, the asymmetry in Figure 4o between top and bottom shows that not only a pure quadrupole is excited. We attribute these effects to a complex interplay between the quadrupole mode and other dipolar modes which are also weakly excited at 800 nm. Further study is required to fully explain the observed angular emission pattern. It is interesting to note that the asymmetry does not arise in the $m = 1$ dipolar emission pattern.

For the $m = 2$ resonance, Figure 6 shows the angular emission at 600 nm for different excitation positions, analogous to the $m = 1$ resonance patterns in Figure 5. Clearly, the angular emission pattern is rotated for different excitation positions along the edge of the center plateau. The bright emission spot at 30° from the normal always points to the direction opposite the electron beam position, confirming that the electron beam position determines the local field symmetries.

Using the angular emission data, the patterns observed in the excitation maps of Figure 4 can now be fully explained. In Figure 4(i) the emission maximum only falls on the slit when the electron beam is positioned at the top or bottom of the ring, hence the two maxima. The upper maximum has a lower intensity, which is because the emission partly falls outside of the mirror acceptance angles. In Figure 4l, there is only a horizontal polarization component in the emission when the electron beam dwells at the left or right, but in this case the emission falls completely outside of the slit. At positions between top, bottom, left and right, a small fraction will fall on the slit with a small horizontal component. Here, four maxima appear. Clearly, when considering the angular emission pattern and the acceptance range of the slit, the polarized experiment provides us with a method to distinguish between mode orders.

The results show that although the same mode is excited at different positions in the resonator, its polarization and far-field emission patterns are very position-dependent. By choosing mode order and excitation position, the far-field emission and polarization of a ring antenna can be fully engineered. This implies that despite their spherical symmetry, plasmonic whispering gallery cavities can be employed to beam emission from light sources embedded in the cavity to nonzero angles.

We have demonstrated that plasmonic whispering gallery resonators are effective optical antennas both in the receiving and transmitting modes. Using spatially, angle- and polarization-resolved cathodoluminescence spectroscopy, we fully resolve the resonant modes, their spatial distribution and polarization resolved emission. We have shown how far-field excitation selectively excites dipolar resonances leading to a Fano line shape in the scattering spectrum. In contrast, electron-beam excitation leads to $m = 0$, 1, 2 dipolar and quadrupolar modes that can be selectively excited. The orientation of the multipolar resonance can be studied by accurately positioning the electron beam. We detect the corresponding angular emission distribution in the far field.

The resonance tunability and control over the mode structure offered by plasmonic whispering gallery resonators offers many possibilities for their use as optical antennas both in the receiving and transmitting mode.

AUTHOR INFORMATION

Corresponding Author

*E-mail: vesseur@amolf.nl.

ACKNOWLEDGMENTS

This work is part of the research program "Microscopy and modification of nanostructures with focused electron and ion beams" (MMN) of the "Stichting voor Fundamenteel Onderzoek der Materie" (FOM), which is financially supported by the "Nederlandse organisatie voor Wetenschappelijk Onderzoek" (NWO). The MMN program is cofinanced by FEI Company. The authors acknowledge F. Javier García de Abajo and Peter J. Nordlander for discussions.

REFERENCES

(1) Bharadwaj, P.; Deutsch, B.; Novotny, L. *Adv. Opt. Photonics* **2009**, *1*, 438−483.
(2) Muskens, O.; Giannini, V.; Sánchez-Gil, J.; Gómez-Rivas, J. *Nano Lett.* **2007**, *7*, 2871−2875.
(3) Ringler, M.; Schwemer, A.; Wunderlich, M.; Nichtl, A.; Kurzinger, K.; Klar, T. A.; Feldmann, J. *Phys. Rev. Lett.* **2008**, *100*, 203002.
(4) Vecchi, G.; Giannini, V.; Rivas, J. G. *Phys. Rev. Lett.* **2009**, *102*, 146807.
(5) Kinkhabwala, A.; Yu, Z.; Fan, S.; Avlasevich, Y.; Mullen, K.; E., M. W. *Nat. Photonics* **2009**, *3*, 654−657.
(6) Mertens, H.; Biteen, J. S.; Atwater, H. A.; Polman, A. *Nano Lett.* **2006**, *6*, 2622−2625.
(7) Kosako, T.; Kadoya, Y.; Hofmann, H. F. *Nat. Photonics* **2010**, *4*, 312−315.
(8) Curto, A. G.; Volpe, G.; Taminiau, T. H.; Kreuzer, M. P.; Quidant, R.; van Hulst, N. F. *Science* **2010**, *329*, 930−933.
(9) Tang, L.; Kocabas, S. E.; Latif, S.; Okyay, A. K.; Ly-Gagnon, D.-S.; Saraswat, K. C.; Miller, D. A. B. *Nat. Photonics* **2008**, *2*, 226−229.
(10) Mertens, H. Controlling plasmon-enhanced luminescence. Ph.D. thesis, FOM Institute for Atomic and Molecular Physics (AMOLF), Utrecht University, Utrecht, The Netherlands, 2007.
(11) Krenn, J.; Schider, G.; Rechberger, W.; Lamprecht, B.; Leitner, A.; Aussenegg, F. *Appl. Phys. Lett.* **2000**, *77*, 3379.
(12) Novotny, L. *Phys. Rev. Lett.* **2007**, *98*, 266802.
(13) Mühlschlegel, P.; Eisler, H. J.; Martin, O. J. F.; Hecht, B.; Pohl, D. W. *Science* **2005**, *308*, 1607.
(14) Muskens, O. L.; Giannini, V.; Sánchez-Gil, J. A.; Rivas, J. G. *Opt. Express* **2007**, *15*, 17736−17746.
(15) Ghenuche, P.; Cherukulappurath, S.; Taminiau, T. H.; van Hulst, N. F.; Quidant, R. *Phys. Rev. Lett.* **2008**, *101*, 116805.
(16) Chu, M.-W.; Myroshnychenko, V.; Chen, C. H.; Deng, J.-P.; Mou, C.-Y.; García de Abajo, F. J. *Nano Lett.* **2009**, *9*, 399−404.
(17) Huang, J.-S.; Kern, J.; Geisler, P.; Weinmann, P.; Kamp, M.; Forchel, A.; Biagioni, P.; Hecht, B. *Nano Lett.* **2010**, *10*, 2105−2110.
(18) Maier, S. A.; Kik, P. G.; Atwater, H. A. *Appl. Phys. Lett.* **2002**, *81*, 1714−1716.
(19) Sweatlock, L. A.; Maier, S. A.; Atwater, H. A.; Penninkhof, J. J.; Polman, A. *Phys. Rev. B* **2005**, *71*, 235408.
(20) Penninkhof, J. J. Tunable plasmon resonances in anisotropic metal nanostructures. Ph.D. thesis, FOM Institute for Atomic and Molecular Physics (AMOLF), Utrecht University, Utrecht, The Netherlands, 2006.
(21) de Waele, R.; Koenderink, A.; Polman, A. *Nano Lett.* **2007**, *7*, 2004−2008.
(22) Bidault, S.; García de Abajo, F. J.; Polman, A. *J. Am. Chem. Soc.* **2008**, *130*, 2750−2751.
(23) Vesseur, E. J. R.; Garca de Abajo, F. J.; Polman, A. *Nano Lett.* **2009**, *9*, 3147−3150.
(24) Vesseur, E. J. R.; de Waele, R.; Kuttge, M.; Polman, A. *Nano Lett.* **2007**, *7*, 2843−2846.
(25) Zhu, X. L.; Ma, Y.; Zhang, J. S.; Xu, J.; Wu, X. F.; Zhang, Y.; Han, X. B.; Fu, Q.; Liao, Z. M.; Chen, L.; Yu, D. P. *Phys. Rev. Lett.* **2010**, *105*, 127402.
(26) Fano, U. *Phys. Rev.* **1961**, *124*, 1866−1878.

(27) Luk'yanchuk, B.; Zheludev, N. I.; Maier, S. A.; Halas, N. J.; Nordlander, P.; Giessen, H.; Chong, C. T. *Nat. Mater.* **2010**, *9*, 707–715.
(28) Coenen, T.; Vesseur, E. J. R.; Polman, A.; Koenderink, A. F. *Nano Lett.* **2011**, *11*, 3779.
(29) Coenen, T.; Vesseur, E. J. R.; Polman, A. *Appl. Phys. Lett.* **2011**, *99*, 143103.
(30) Garca de Abajo, F. J. *Rev. Mod. Phys.* **2010**, *82*, 209–275.
(31) Novotny, L.; Hecht, B. *Principles of Nano-Optics*; Cambridge University Press: Cambridge, 2006.
(32) Jackson, J. *Classical Electrodynamics*; Wiley: New York, 1999.
(33) Encina, E. R.; Coronado, E. A. *J. Phys. Chem. C* **2008**, *112*, 9586–9594.